NEW DYE FOR AMYLOID STAINING

Showcasing research from the laboratories of Professor Borys Ośmiałowski (Nicolaus Copernicus University, Poland) and Professor Joanna Olesiak-Bańska (Wrocław University of Science and Technology, Poland).

A novel *O,N,O*-coordinated organofluoroboron probe for amyloid detection: insight from experiment and theory

This work reports on a newly synthesized BF-based organoboron dye exhibiting good optical properties, including fluorescence reaching the NIR-I region, two-photon absorption in the NIR-II region, a broad excitation range and high increment of emission intensity upon binding to amyloids.

Image reproduced by permission of Elizaveta F. Petrusevich and Borys Ośmiałowski from *Chem. Commun.*, 2025, **61**, 3990.

Elizaveta F. Petrusevich is acknowledged for creation of the image.

As featured in:

See Robert Zaleśny, Borys Ośmiałowski, Joanna Olesiak-Bańska *et al.*, *Chem. Commun.*, 2025, **61**, 3990.

ROYAL SOCIETY OF CHEMISTRY

rsc.li/chemcomm

Check for updates

A novel *O,N,O*-coordinated organofluoroboron probe for amyloid detection: insight from experiment and theory†

Agata Hajda, [a] Elizaveta F. Petrusevich, [b] Robert Zaleśny, *[a] Borys Ośmiałowski *[c] and Joanna Olesiak-Bańska *[a]

This work presents the results of photophysical studies for a newly synthesized BF-based organoboron dye of D–A–D topology. The one- and two-photon properties of the dye are compared with the D–A parent compound and commercially available amyloid marker: methoxy-X04. We demonstrate that the new dye exhibits better optical properties upon binding to amyloids than methoxy-X04, including emission above 600 nm, higher values of 2PA cross section, broader excitation range and higher increment of emission intensity upon binding to amyloids. All these data demonstrate that the new probe is an interesting scaffold for application in two-photon microscopy and amyloid staining.

Fluorescent probes exhibiting red and near infra-red (NIR) excitation and emission are in high demand due to their potential in bioimaging. The irradiation wavelengths corresponding to biological windows (>700 nm) provide deeper penetration into the sample, improve contrast and safeguard lower phototoxicity.[1,2] A viable route to use irradiation wavelengths matching biological windows is two-photon microscopy (2PM), as this technique relies on the simultaneous absorption of two photons. In the case of degenerate two-photon absorption (2PA) process photon energies are equal so in 2PM the excitation occurs at two times longer wavelengths in comparison to a one-photon absorption process.[3] The design of fluorophores, which might serve as potential novel two-photon probes, is by far a nontrivial process as the tuning of the photophysical properties (fluorescence quantum yield (FQY, Φ), excitation/emission wavelength ($\lambda_{EX}/\lambda_{EM}$), and 2PA cross-section (σ_2)) needs to be addressed in a holistic way

(multiparameter optimization). 2PM is a widely used technique in the imaging of complex deep-laying structures, *e.g.*, in the detection of amyloid plaques in the brain.[4–6] The mentioned amyloids are aggregates of misfolded proteins and peptides. Their presence can be associated with various diseases, especially neurodegenerative ones, such as Alzheimer's disease, but also type 2 diabetes. The palette of fluorescent probes for amyloid detection used in 2PM is much more narrow, compared to one-photon microscopy (1PM). Recently, several imaging agents specifically designed for 2PM have been developed, featuring red/NIR emission, appropriate σ_2 values, and high affinity for amyloids.[7,8] There is a piece of evidence[9–12] that probes with improved properties (high FQY and σ_2, $\lambda_{EM} > 600$ nm) can provide additional information, compared to the widely used two-photon standard in amyloid staining, such as methoxy-X04 (MeO-X04), in which λ_{EM} is shorter than 550 nm.[12,13] However, progress in the development of two-photon probes for amyloids remains limited compared to one-photon probes, making each proposed 2PM agent a valuable research tool.

A promising platform for the design of two-photon-excited fluorescent probes for 2PM is the one composed of organoboron complexes carrying BF/BF₂ moieties. Since the (bis)fluoroborate group is a strong acceptor of electrons, it can be combined with electron-donating moieties, yielding dipolar (non-centrosymmetric) or quadrupolar (centrosymmetric) dyes suitable for efficient 2PA with excellent remaining photophysical properties.[14] Dyes exhibiting intramolecular charge transfer (ICT) upon electronic excitation that are sensitive to environment or structural changes are natural candidates as fluorescent probes, *e.g.*, for amyloid staining. In this work we rely on the previous findings by Chen *et al.*, demonstrating the usefulness of BF₂-carrying donor–acceptor (D–A) dyes in β-amyloid and tau tangle staining,[15,16] and propose the D–A to D–A–D topology extension (see Fig. 1). In doing so, we aim at the red-shift of the emission wavelength and the enhancement of the interaction with bio-molecules by two *N,N*-dimethylamino (NMe₂) groups, as the interaction *via* an amino moiety was proven to be responsible for binding with amyloid fibrils.[17]

[a] *Faculty of Chemistry, Wroclaw University of Science and Technology, Wybrzeże Wyspiańskiego 27, 50-370 Wrocław, Poland. E-mail: robert.zalesny@pwr.edu.pl, joanna.olesiak-banska@pwr.edu.pl*

[b] *Faculty of Chemistry, University of Gdańsk, Fahrenheit Union of Universities in Gdańsk, Wita Stwosza 63, 80-308 Gdańsk, Poland*

[c] *Faculty of Chemistry, Nicolaus Copernicus University, Gagarina 7, PL-87100 Toruń, Poland. E-mail: borys.osmialowski@umk.pl*

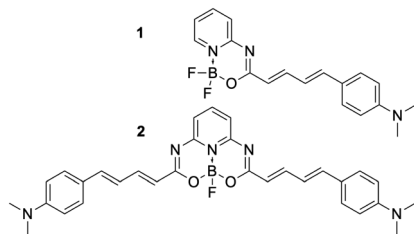† Electronic supplementary information (ESI) available. See DOI: https://doi.org/10.1039/d5cc00243e

Fig. 1 The structure of molecules studied in the present work.

Table 1 Experimental spectroscopic data for dyes in $CHCl_3$ – extinction coefficient (ε), absorption (λ_{ABS}) and emission (λ_{EM}) wavelength, fluorescence quantum yield (FQY), fluorescence lifetime (τ) and its amplitude (α)

Dye	ε [M^{-1} cm^{-1}]	λ_{ABS} [nm]	λ_{EM} [nm]	FQY [%]	τ [ns]
1	48 000	460.5	595	9.8	0.641^a
2	47 800	436, 494	620	22.0	0.829

^{a} τ_{ave}: $\tau_1 = 0.055$ ns, $\alpha = 12.91$; $\tau_2 = 0.728$ ns, $\alpha = 87.09$.

Note that heterocyclic cores in **1** and **2** are substituted with identical terminal moieties (''arms''). We will compare the effectiveness of staining model amyloids obtained from bovine insulin by these two dyes.

Synthesis, experimental and computational details are described in the ESI† (see, *e.g.*, Fig. S1–S5). One-photon properties (1P) like 1PA (Fig. 2), one-photon excited fluorescence (1PEF), FQY, and fluorescence lifetimes (τ) of both dyes in $CHCl_3$ were acquired, which is summarized in Table 1 (for **1** in agreement with previous data[18]) and more detailed data are presented in the ESI.† Spectra of 1PEF in $CHCl_3$, and additionally in DMSO are presented in Fig. S6 in the ESI.† The absorption and the emission spectra of **1** (see Fig. 2A and Fig. S6A, ESI†) present mirror-like images, suggesting a relatively limited geometrical relaxation of the Franck–Condon singlet excited state. However, in the case of **2** (see Fig. 2B and Fig. S6B, ESI†) the mirror-image rule does not hold (similarly to the smaller molecule carrying the same core[18]) because two, close in energy bands in the absorption spectra between 400–600 nm correspond to two electronic states (see below for the analysis of electronic-structure calculations). For 1PA and 1PEF, a bathochromic shift of the broadened bands, caused by the flexibility of π-conjugated arms, was observed for **2** as compared to **1**. This phenomenon is accompanied by an over double increase in FQY (Table 1). Enhancement of FQY is highly beneficial for fluorophores with red-shifted emission. According to the energy-gap rule, the emission efficiency drops down as the energy between the ground and excited state decreases, which means that the far-red emitting dyes are usually much less efficient in comparison with their counterparts showing emission in the blue part of the spectrum. The radiative (k_r) rate constant for **2** (2.65×10^8 s^{-1}) is higher than that for **1** (1.53×10^8 s^{-1}); conversely, the non-radiative (k_{nr}) rate constant for **1** (1.41×10^9 s^{-1}) is larger

than that for **2** (9.41×10^8 s^{-1}), which can be linked with the topologies of BF/BF_2-carrying cores (compare ref. 18). We measured the 2PA spectra using the two-photon excited fluorescence (2PEF) method, and we further supported these measurements by electronic-structure calculations. The palette of simulated properties (*vide infra*) encompasses excitation energies, oscillator strengths, Ciofini's charge transfer diagnostics, electronic density difference plots and two-photon transition strengths (see the ESI,† Fig. S20–S24 and Tables S2, S3). The non-linear nature of the observed processes was determined based on the quadratic dependence of photoluminescence intensity on the incident laser power confirming two-photon absorption (Fig. S7C and D, ESI†). For dye **1**, the 2PA band matches the 1PA band (Fig. 2A). The peak values of σ_2 for **1** at 920 nm reach 700 GM and the band maxima are red-shifted compared to the results of simulations (Table 2), which comes as no surprise given the predictive power of the employed coupled-cluster model. The results of electronic-structure calculations demonstrate higher values of σ_2 for $S_0 \rightarrow S_1$, than for $S_0 \rightarrow S_2$, which comes from the larger difference in dipole moment between the excited and the ground state. It should be noted that the calculated 2PA cross section for the $S_0 \rightarrow S_1$ transition satisfactorily matches the value measured experimentally (Fig. 2A). Note that the estimation of 2PA experimentally in the regime of higher energy transition ($S_0 \rightarrow S_2$) was unsuccessful, due to the emission wavelength overlapping with the excitation wavelength. Molecule **2** presents two absorption maxima in 1PA, which is also visible in the 2PA spectrum (Fig. 2B). However, the σ_2 value at 880 nm with 1101 GM is much more prominent than the value of σ_2 equal to 400 GM at 1020 nm. The results of calculations demonstrate that the σ_2 value for $S_0 \rightarrow S_2$ is roughly 20 times larger than that calculated for $S_0 \rightarrow S_1$. Note that due to close proximity of the absorption bands, the experiment-theory comparison of σ_2 for $S_0 \rightarrow S_1$ is difficult as both transitions contribute to the 2PA cross section value at
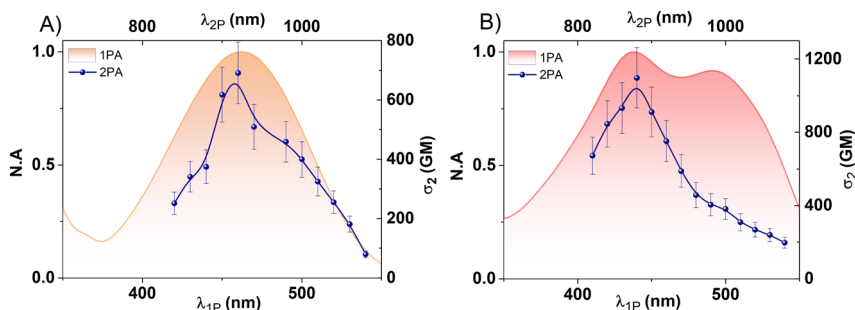

Fig. 2 Normalized one-photon absorption spectra and two-photon absorption spectra (in GM) of molecules **1** (A) and **2** (B).

Table 2 Spectroscopic properties (one-photon excitation energy (ΔE) and wavelength (λ), dipole moment (μ), two-photon transition strength (δ^{2PA})) and two-photon absorption cross section (σ_2) calculated at the RI-CC2/def2-TZVP/EE level of theory for **1** and **2** in CHCl$_3$

	Transition	ΔE [eV]	λ [nm]	f	$\Delta\mu$ [D]	$\mu(S_n)$ [D]	δ^{2PA} [a.u.]	σ_2 [GM]
1	$S_0 \rightarrow S_1$	3.00	414	1.85	14.1	23.6	188×10^3	494
	$S_0 \rightarrow S_2$	4.04	307	0.04	4.8	14.3	37×10^3	176
2	$S_0 \rightarrow S_1$	2.84	437	3.04	3.8	8.8	32×10^3	75
	$S_0 \rightarrow S_2$	3.17	392	0.40	4.2	9.2	492×10^3	1442

1020 nm (*cf.* Fig. 2B and Table 2). Comparing both dyes, one finds that maximal two-photon absorption action cross-section $\sigma_{2,eff}$ ($\sigma_2 \times \Phi$) is higher for **2**, which implies greater potential in imaging applications. A closer look at two-photon excitation above 1000 nm shows $\sigma_{2,eff} > 50$ GM, which is still an effective value for application of **2** as a fluorescent probe in the NIR-II window.[19]

In order to further understand the two-photon activity of **1** and **2** we performed the analysis based on the generalized few-state model for theories with a non-Hermitian structure.[20] The summary of these calculations is shown in Fig. 3, which presents the two-photon transition strengths (δ^{2PA}) computed by response theory as well as based on two- and three-state models. Note that δ^{2PA} is a purely molecular parameter and it is proportional to σ_2 (see eqn (S3) in the ESI†). In more detail, we aimed at explaining the differences in two-photon absorption activity between **1** ($S_0 \rightarrow S_1$) and **2** ($S_0 \rightarrow S_2$). In the case of **1**, the two-state model yields the values of two-photon $S_0 \rightarrow S_1$ transition strengths similar to that from response theory calculations and the extension to the three-state model (by including S_2 state as the intermediate) leads
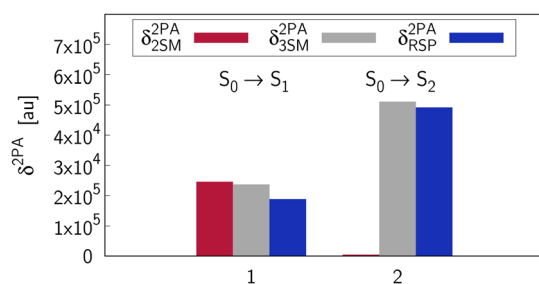

Fig. 3 Two-photon transition strengths predicted by response theory (RSP), and the two- (2SM) and three-state model (3SM) for **1** and **2**.

to insignificant improvement. In other words, the parameters of the ground and final state (energy difference, transition strength and dipole moment difference) determine the two-photon $S_0 \rightarrow S_1$ activity of molecule **1**. On the other hand, the same is not true for two-photon $S_0 \rightarrow S_2$ transition for **2**, *i.e.*, the two-state model (including ground and the final state S_2) fails to reproduce the two-photon $S_0 \rightarrow S_2$ transition strength. It is necessary to go beyond the two-state model to reproduce the response theory value. The three-state model that yields satisfactory agreement with response theory includes the ground, final (S_2) and intermediate state (S_1). One may thus conclude that the differences in two-photon absorption activity between **1** ($S_0 \rightarrow S_1$) and **2** ($S_0 \rightarrow S_2$) are due to very different physical mechanisms and the latter property depends on the coupling between S_1 and S_2 states.

Dye **1** was previously evaluated as a fluorescent probe for amyloid staining and showed various responses upon binding to Aβ and tau amyloids.[15] Therefore, studying interaction with amyloids for dye **2** seems well justified, especially since it has λ_{EM} shifted towards the red part of the spectrum and high $\sigma_{2,eff}$ in the NIR-I (700–950 nm) and NIR-II (>1000 nm) biological windows. Here, we compared the optical properties of dye **1**, dye **2** and MeO-X04 – a fluorescent standard commonly used for amyloid staining in 2PM[13,21,22] – upon binding to bovine insulin amyloids. Insulin serves as a good model system since it forms uniform fibrils, which was confirmed by atomic force microscopy (AFM) and transmission electron microscopy (TEM) analysis (see Fig. S9 and S10, ESI†). Photophysical parameters of MeO-X04 upon binding to amyloids like 1PA, 1PEF, 1PE (one-photon excitation) and σ_2 are rarely discussed in the literature.[12] Our experiments can also shed light on the 1P and 2P properties of this probe. For all considered molecules (dye **1**, dye **2** and MeO-X04), fluorescence was measured as a function of increasing amyloid concentration (Fig. S11 in ESI†). The highest fluorescence enhancement was observed for dye **2**, while the lowest one for MeO-X04, which is presented in Fig. 4A. λ_{EM} with amyloids of dye **1** (623 nm) and dye **2** (627 nm) are significantly bathochromically shifted from the spectra of MeO-X04, which presents several maxima due to the vibrational fine structure (427 nm; 454 nm; 484 nm) of Fig. 4B. The emission between 400–500 nm falls into ranges where autofluorescence, absorption and scattering of tissues dominates, which can significantly influence its performance, which was proven during *in vivo* imaging analysis.[11,23] It is worth pointing
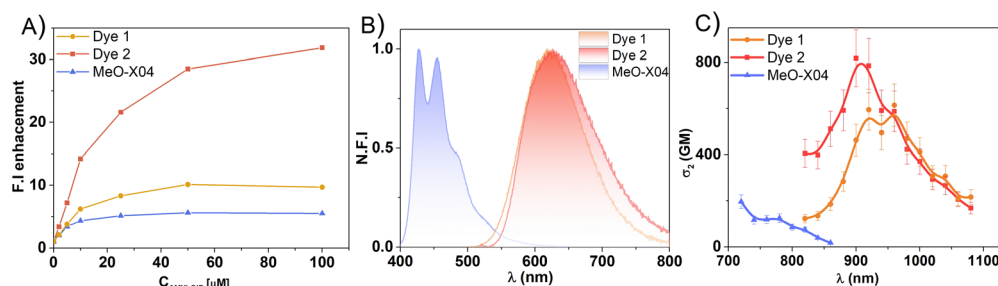

Fig. 4 (A) Increase in fluorescence maximum upon adding bovine insulin amyloids; all dyes had 0.5 μM, and the solvent was 5% DMSO. Point "zero" was the dye in 5% DMSO without amyloids; (B) comparison of normalized 1PEF for all dyes (1 μM) with 50 μM of bovine insulin amyloids. The same solutions were taken for 2PEF measurements; (C) comparison of σ_2 with 50 μM of amyloids.

out that dye **2** has even more prominent emission above 700 nm than dye **1**, which can be seen in Fig. 4B. The bathochromic shift in λ_{EM} of the dye **2** observed in solvents with increasing polarity (see Fig. S12 in ESI†) suggests that the molecule is located in the more hydrophobic regions of the amyloid fibrils. It is also supported by the value of FQY in amyloids (10%), which is much higher than in polar DMSO (0.6%) – see Table S1 in the ESI.† Additionally, dye **2** is substituted by NMe_2 groups at both arms and it contains single C–C bonds that can easily rotate or kink leading to non-radiative energy dissipation. Upon binding to amyloids, NMe_2 groups can have restricted conformational freedom, which is observed as fluorescence enhancement. We can observe a significant difference in 1PE upon increasing the amyloid concentration for dye **2** (see Fig. S13 in the ESI†). 1PE changes the shape of the spectrum; the band around 450 nm starts to vanish, and a new band around 550 nm starts to appear. No changes in 1PE were observed for dye **1**. In addition, we measured 1PE for MeO-X04, which is presented in Fig. S13C in the ESI.† Additional experiments for dye **2** were conducted due to its novelty. Lack of observed changes in emission between the solution of **2** and upon mixing with insulin monomers, proves interaction with fibrils and not with the native peptide (Fig. S14, ESI†). The affinity of dye **2** (K_d) to insulin amyloids was measured by saturation binding assay. The K_d value was determined to be 229 ± 12 nM (Fig. S15, ESI†). Furthermore, selectivity measurements of dye **2** show the highest fluorescence intensity upon binding to insulin amyloids (Fig. S16, ESI†) compared to other bio-molecules.

The evaluation of the 1P properties was followed by studies of σ_2 upon binding to amyloids. We confirmed the two-photon nature of the observed process (see Fig. S17C and D, ESI†). No alteration in λ_{EM} was observed upon two-photon excitation (2PE) compared to 1PE for dye **1** and dye **2** (Fig. S18, ESI†) indicating relaxation from the same energy state. Evaluation of σ_2 revealed that dye **2** upon binding has the highest 2PA among all dyes (Fig. 4C), which is in line with the trend in $CHCl_3$. The lowest values of 2PA are found for MeO-X04, and these were measured within the 720–860 nm range (Fig. 4C). At longer wavelengths of 2PE, no emission was detected in the used experimental conditions. On the other hand, 2PE for dye **1** and dye **2** have a much broader range overlapping with both the NIR-I and NIR-II biological window, which is beneficial from an application point of view. The detailed comparison of 1PA and 2PA upon binding is presented in the ESI† (Fig. S19).

To sum up, newly synthesized dye **2** has better optical properties upon binding to amyloids than MeO-X04, including emission spectra above 600 nm, higher values of 2PA cross section, and broader excitation range in both the NIR-I and NIR-II biological window. We also proved that the branched architecture (D–A–D) has higher σ_2 upon binding to amyloids, compared to their unsymmetrical parent compound (D–A). The newly synthesized compound **2** also exhibits a higher increment of emission intensity upon binding to amyloids. All these data demonstrate that the new probe is an interesting scaffold for further development for applications in 2PM and amyloid detection.

Data availability

The data supporting this article have been included as part of the ESI.†

Conflicts of interest

There are no conflicts of interest.

Notes and references

1 G. Hong, A. L. Antaris and H. Dai, *Nat. Biomed. Eng.*, 2017, **1**, 0010.
2 R. Weissleder, *Nat. Biotechnol.*, 2001, **19**, 316–317.
3 A. M. Larson, *Nat. Photon.*, 2011, **5**, 1.
4 S. Burgold, S. Filser, M. M. Dorostkar, B. Schmidt and J. Herms, *Acta Neuropathol. Commun.*, 2014, **2**, 30.
5 P. d'Errico, S. Ziegler-Waldkirch, V. Aires, P. Hoffmann, C. Mezö, D. Erny, L. S. Monasor, S. Liebscher, V. M. Ravi, K. Joseph, O. Schnell, K. Kierdorf, O. Staszewski, S. Tahirovic, M. Prinz and M. Meyer-Luehmann, *Nat. Neurosci.*, 2022, **25**, 20–25.
6 S. Burgold, T. Bittner, M. M. Dorostkar, D. Kieser, M. Fuhrmann, G. Mitteregger, H. Kretzschmar, B. Schmidt and J. Herms, *Acta Neuropathol.*, 2011, **121**, 327–335.
7 L. Li, Z. Lv, Z. Man, Z. Xu, Y. Wei, H. Geng and H. Fu, *Chem. Sci.*, 2021, **12**, 3308–3313.
8 M. Chen, Z. Zhang, Z. Shi, J. Sun and F. Gao, *Cell Rep. Phys. Sci.*, 2024, **5**, 101810.
9 D. Kim, H. Moon, S. H. Baik, S. Singha, Y. W. Jun, T. Wang, K. H. Kim, B. S. Park, J. Jung, I. Mook-Jung and K. H. Ahn, *J. Am. Chem. Soc.*, 2015, **137**, 6781–6789.
10 J.-W. Choi, Y. H. Ju, Y. Choi, S. J. Hyeon, C. G. Gadhe, J.-H. Park, M. S. Kim, S. Baek, Y. Kim, K. D. Park, A. N. Pae, H. Ryu, C. J. Lee and B. R. Cho, *ACS Chem. Neurosci.*, 2020, **11**, 1801–1810.
11 C. Chen, Z. Liang, B. Zhou, X. Li, C. Lui, N. Y. Ip and J. Y. Qu, *ACS Chem. Neurosci.*, 2018, **9**, 3128–3136.
12 C. H. Heo, K. H. Kim, H. J. Kim, S. H. Baik, H. Song, Y. S. Kim, J. Lee, I. Mook-jung and H. M. Kim, *Chem. Commun.*, 2013, **49**, 1303–1305.
13 W. E. Klunk, B. J. Bacskai, C. A. Mathis, S. T. Kajdasz, M. E. McLellan, M. P. Frosch, M. L. Debnath, D. P. Holt, Y. Wang and B. T. Hyman, *J. Neuropathol. Exp. Neurol.*, 2002, **61**, 797–805.
14 M. Pawlicki, H. Collins, R. Denning and H. Anderson, *Angew. Chem., Int. Ed.*, 2009, **48**, 3244–3266.
15 Y. Chen, Q. Ouyang, Y. Li, Q. Zeng, B. Dai, Y. Liang, B. Chen, H. Tan and M. Cui, *Eur. J. Med. Chem.*, 2022, **227**, 113968.
16 Y. Chen, C. Yuan, T. Xie, Y. Li, B. Dai, K. Zhou, Y. Liang, J. Dai, H. Tan and M. Cui, *Chem. Commun.*, 2020, **56**, 7269–7272.
17 K. J. Robbins, G. Liu, G. Lin and N. D. Lazo, *J. Phys. Chem. Lett.*, 2011, **2**, 735–740.
18 A. M. Grabarz, A. D. Laurent, B. Jędrzejewska, A. Zakrzewska, D. Jacquemin and B. Ośmiałowski, *J. Org. Chem.*, 2016, **81**, 2280–2292.
19 H. M. Kim and B. R. Cho, *Chem. Rev.*, 2015, **115**, 5014–5055.
20 M. T. P. Beerepoot, M. M. Alam, J. Bednarska, W. Bartkowiak, K. Ruud and R. Zaleśny, *J. Chem. Theory Comput.*, 2018, **14**, 3677–3685.
21 D. S. Whittaker, L. Akhmetova, D. Carlin, H. Romero, D. K. Welsh, C. S. Colwell and P. Desplats, *Cell Metab.*, 2023, **35**, 1704–1721.
22 M. Meyer-Luehmann, T. L. Spires-Jones, C. Prada, M. Garcia-Alloza, A. de Calignon, A. Rozkalne, J. Koenigsknecht-Talboo, D. M. Holtzman, B. J. Bacskai and B. T. Hyman, *Nature*, 2008, **451**, 720–724.
23 J. Shin, P. Verwilst, H. Choi, S. Kang, J. Han, N. H. Kim, J. G. Choi, M. S. Oh, J. S. Hwang, D. Kim, I. Mook-Jung and J. S. Kim, *Angew. Chem., Int. Ed.*, 2019, **58**, 5648–5652.